Available online at www.sciencedirect.com
ScienceDirect
International Journal of Multiphase Flow 34 (2008) 312–321
International Journal of Multiphase Flow
www.elsevier.com/locate/ijmulflow

NMR imaging of fluid pathways during drainage of softwood in a pressure membrane chamber

G. Almeida [a], S. Leclerc [b], P. Perre [c,*]

[a] Laboratório de Química, Celulose e Energia, Escola Superior de Agricultura "Luiz de Queiroz", Universidade de São Paulo (ESALQ/USP), Av. Pádua Dias, 11 CP 9 Piracicaba, Brazil

[b] Laboratoire d'Énergétique et de Mécanique Théorique et Appliquée (LEMTA), UMR 7563 CNRS – Nancy Université, INPL, BP 160, Vandoeuvre-les-Nancy, France

[c] Laboratoire d'Etudes et de Recherche sur le Matériau Bois (LERMAB), UMR INRA/ENGREF/UHP 1093, ENGREF, 14 rue Girardet, Nancy, France

Received 22 June 2007; received in revised form 21 September 2007

Abstract

An experiment was implemented to study fluid flow in a pressure media. This procedure successfully combines nuclear magnetic resonance imaging with a pressure membrane chamber in order to visualize the non-wetting and wetting fluid flows with controlled boundary conditions. A specially designed pressure membrane chamber, made of non-magnetic materials and able to withstand 4 MPa, was designed and built for this purpose. These two techniques were applied to the drainage of Douglas fir sapwood. In the study of the longitudinal flow, narrow drainage fingers are formed in the latewood zones. They follow the longitudinal direction of wood and spread throughout the sample length. These fingers then enlarge in the cross-section plane and coalesce until drainage reaches the whole latewood part. At the end of the experiments, when the drainage of liquid water in latewood is completed, just a few sites of percolation appear in earlywood zones. This difference is a result of the wood anatomical structure, where pits, the apertures that allow the sap to flow between wood cells, are more easily aspirated in earlywood than in latewood.

Keywords: NMR imaging; Pressure membrane; Porous media; Douglas fir; Multiphase flow; Percolation network

1. Introduction

To understand the mechanisms affecting the fluid flow in a porous media is very important for several applications such as drying and impregnation processes. Wood is a representative example of porous media, whose cellular structure is composed by a pore network joined by narrower connecting throats (pits). Softwood species have much greater uniformity than hardwoods. The principal structure of softwoods is the longitudinal tracheids, with approximately 92% of the volumetric composition. Tracheid size varies according to the species, the position in the tree and the kind of wood. In general, these elements have an average length of about 3500 μm and an average cross-sectional diameter of about 30 μm (Panshin and de Zeeuw, 1980). Due to wood physiology, tracheids formed during summer (latewood) have cell walls much thicker than those formed during spring (earlywood). Indeed, the double cell wall increases from about 4 μm in earlywood to more than 10 μm in latewood. This difference affects its physical and mechanical properties greatly. Tracheids are connected by bordered pits, which consist of two complementary gaps or recesses in the cell walls. These pits are covered with a membrane much thinner than the rest of the cell wall called the torus. The torus is surrounded by the annular margo consisting of microfibrillar strands with openings between them permitting the passage of liquids between the cells (Core et al., 1979; Panshin and de Zeeuw, 1980; Siau, 1995). If a gas/liquid interface passes through

* Corresponding author. Tel.: +33 3 83 39 68 90; fax: +33 3 83 39 68 47.
E-mail addresses: almeida@nancy-engref.inra.fr (G. Almeida), Sebastien.Leclerc@rmn.uhp-nancy.fr (S. Leclerc), perre@nancy-engref.inra.fr (P. Perre).

0301-9322/$ - see front matter © 2007 Elsevier Ltd. All rights reserved.
doi:10.1016/j.ijmultiphaseflow.2007.10.009

the pit, the capillary forces cause the membrane to move into the aspirated position, closing off the water flow. In the living tree, this feature exists to limit the damage due to cavitation in the sap column. In the case of wood as a material pit aspiration inhibits the liquid flow and is often problematic (drying and preservation).

Nuclear magnetic resonance imaging (MRI) is a non-destructive and a non-invasive technique that has been widely used to determine moisture distribution and fluid flow through a porous medium. For example, MRI has been used to study the flow through a porous medium in many fields including ground water hydrology, petroleum engineering, and soil science (Williams et al., 1991; Waggoner and Fukushima, 1996; Kimmich et al., 2001; Chen et al., 2002; Deurer et al., 2002). The majority of these works study the displacement of two immiscible fluids using a reference liquid and/or glass beads to simulate the porous medium. For example, Chen et al. (2002) used a model consisting of artificially consolidated sandstone saturated with oil. Oil in the model was flooded by an aqueous paramagnetic ion solution (500 mg L^{-1} of $MnCl_2$) at a constant flux of 0.25 mL min^{-1} and the distribution of the two phases at different stages of the water flooding was determined. A column filled with glass beads was used to study water flow in porous media by Deurer et al. (2002). In this study, water was pumped through the glass beads with a Pharmacia double syringe pump at rates of 125 and 250 mL h^{-1}.

Wood can be successfully imaged by MRI because of its relatively regular porous structure, in particular thanks to its almost self-similar structure obtained by a translation in the longitudinal direction. According to Araujo et al. (1993), NMR signal from green wood may be separated into three major components: solid wood, cell-wall water and lumen water. The transversal relaxation time (T_2) of solid wood decays rapidly to zero in tens of microseconds making it readily separable from the cell-wall water (bound water) signal, which has a T_2 from one to a few milliseconds. In contrast, the lumen water (liquid water) has a T_2 ranging from tens to hundreds of milliseconds (Riggin et al., 1979; Menon et al., 1987; Araujo et al., 1993; Almeida et al., 2007). Several works have used this technique to separate sapwood from heartwood, to differentiate growth rings and to visualise internal defects or anomalies of wood (Kuroda et al., 2006; Eberhardt et al., 2006). MRI was also used for non-invasive qualitative and quantitative studies of water distribution in wood and wood-drying kinetics (Quick et al., 1990; Meder et al., 2003; van Houts et al., 2004; Merela et al., 2005).

During experiment of fluid flow in porous media, the accurate control of the boundary conditions is a difficult task, especially at high humidity levels. The present work uses the pressure membrane principle to study the water flow in wood at high relative humidities. Although this method is mostly used on soil science (ASTM, 2000), it has been successfully used by many researchers in the studies of wood–water relationships (Robertson, 1965; Stone and Scallan, 1967; Griffin, 1977; Fortin, 1979; Almeida and Hernández, 2006).

The present work combines MRI with an accurate method to control the drainage inside a porous medium (Douglas fir). This combination permits the displacement of the wetting phase by an overpressure of the non-wetting phase to be observed. The 3D images of the moisture content fields versus time provide new insights into fluid migration mechanisms taking place in softwood: cluster formation, coalescence of cluster, absence of liquid migration in earlywood. To our knowledge, this is the first time that these phenomena have been observed by non-destructive methods and with the rigorous control of drainage conditions.

2. Materials and methods

The study was carried out in 21-year-old Douglas fir (*Pseudotsuga menziesii*). Douglas fir sapwood samples were cut from a green log. Longitudinal and radial specimens were turned using a lathe (Fig. 1A). A diamond wire saw (Well model 3241, ESCIL) was used to cut the cylindrical samples. The final dimensions of the longitudinal specimens were 17 mm in diameter and 20 mm in length (parallel to the longitudinal tracheids) and for the radial ones 17 mm in diameter and 15 mm in length (parallel to the radial elements). In order to maintain the green state until the test, the samples were soaked in distilled water for no more than 10 days. The test material had an average basic wood density (oven-dry mass to green volume) of 467 kg m^{-3} (coefficient of variation (CV) of 5%).

2.1. Experiments

2.1.1. Pressure membrane principle

The pressure membrane principle is used to control the water state in a porous medium at high humidity levels (>95% RH) or to apply a pressure difference between the wetting phase and the non-wetting phase. This principle lies in the concept of water potential (ψ), which is derived from classical thermodynamics and defined as the difference between the specific Gibbs free energy of water in the state under study and in a standard reference state (Siau, 1995). The reference state generally used is a hypothetical pool of pure free water at atmospheric pressure, at a given elevation and at the same temperature as that of the water in the porous material (Fortin, 1979). The water potential is normally expressed in terms of energy per unit mass in J kg^{-1}. The water potential of moist air may be deduced from Kelvin's law.

$$\psi = \frac{RT \ln h}{M_w} \tag{1}$$

where R is the gas constant (8.31 J mol^{-1} K^{-1}); T is the absolute temperature (K); h is the relative vapor pressure and M_w is the molar mass of water (18×10^{-3} kg mol^{-1}).

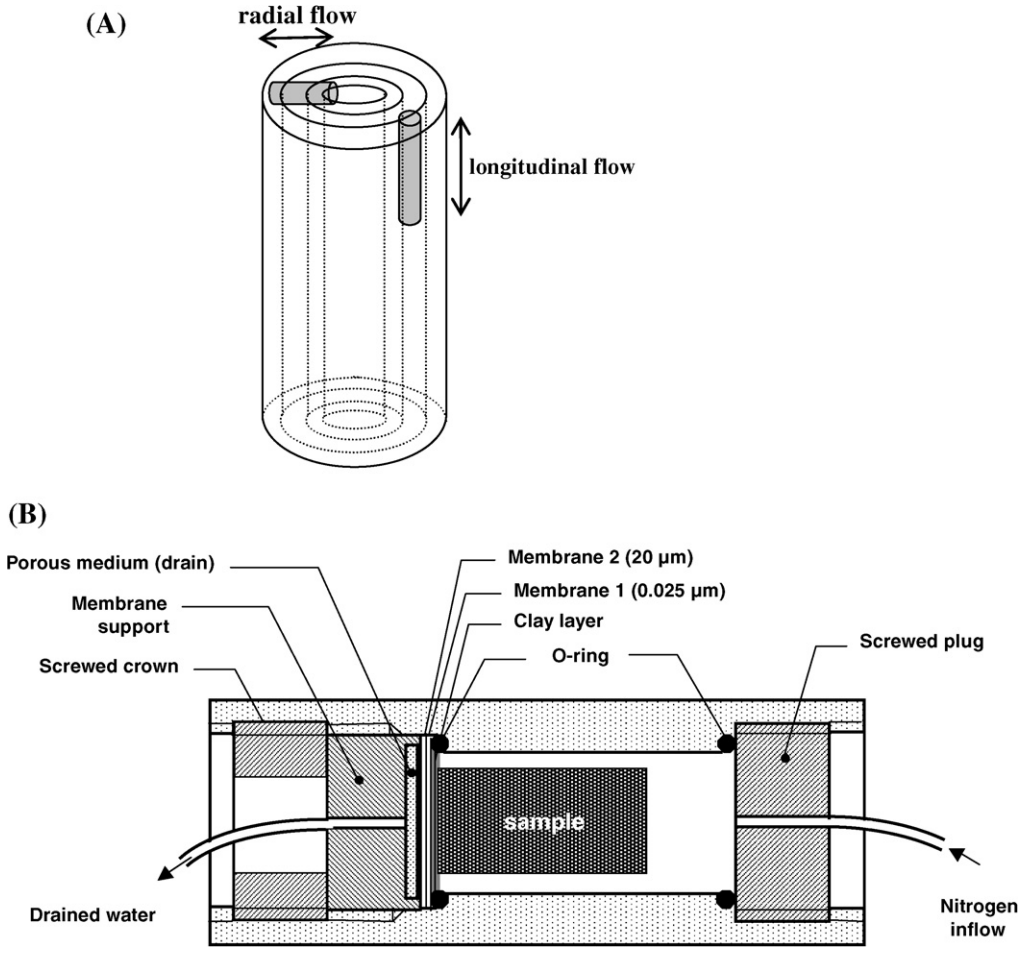

Fig. 1. (A) Diagram of sample placement in the wood stem. (B) Diagram of the pressure chamber used in the pressure membrane/MRI tests.

Eq. (1) relates the relative humidity and the pressure difference between liquid and gas. From this equation, the equivalent radius of curvature of the air–water meniscus can be calculated using Laplace's law. This equivalent radius r is defined by the radius of a cylindrical tube which produces the same pressure difference:

$$r = \frac{-2\gamma\cos\theta}{\rho_w \psi} \tag{2}$$

where γ is the surface tension of the water/air interface (0.072 N m^{-1} at 25 °C), θ is the contact angle between the liquid and the surface of the capillary (0° for a perfectly wetting fluid) and ρ_w is the normal density of water (kg m^{-3}).

A pressure chamber, integrally made of non-magnetic and dielectric materials, was specially designed in order to make the use of the pressure membrane principle inside the NMR spectrometer possible (Fig. 1B). This chamber was designed for a maximal capacity of 4 MPa. Nitrogen pressure was controlled by manometers, which are connected to the pressure chamber by a 1.6 mm diameter Teflon tube.

The longitudinal or radial samples were placed into the pressure chamber on two saturated membranes of different pore diameters (membrane 1 = 20 μm; membrane 2 = 0.025 μm) (Fig. 1B). The solely role of membrane 1, with coarse pores, is to protect the active membrane. The latter effectively withstands the pressure chamber. The system works until the pressure remains below the percolation pressure of the membrane. The one we used, with a diameter of 0.025 μm, is able to operate up to about 10 MPa at 25 °C. A saturated clay layer of about 1 mm thick was placed on membrane 2 in order to ensure hydraulic contact with the specimen. Pressure was then gradually applied until the required level was reached. A maximal pressure of 500 kPa was applied in this work. At this pressure, capillaries with a radius larger than 0.288 μm are emptied (Eq. (2)). Specimens were weighed before and after the pressure membrane/MRI experiments and were oven-dried at 102 °C until equilibrium to determine the moisture content.

2.1.2. MRI analysis

Magnetic resonance imaging experiments were carried out on a Bruker Biospec 24/40 spectrometer equipped with a custom made gradient coil and a 3.5 cm diameter resonator. The pressure chamber was designed to fit precisely into this probe thus avoiding vibration artifacts during the experiment.

Relaxation times in saturated parts of wood were measured using inversion recovery method for longitudinal relaxation time (T_1) and Carr Purcell Meiboon Gill method for transverse relaxation time (T_2). The values measured were 240 ms for T_1 and 37 ms for T_2, which is in agreement with the literature data.

Images were acquired using classical multi-slice spin-echo experiments with the following parameters: repetition time (TR): 1 s, echo time (TE): 18.3 ms, field of view (FOV): 4 cm, matrix: 256 × 192 points, spatial resolution 156 × 208 μm. The repetition time TR was chosen sufficiently long to avoid longitudinal relaxation contrast. TE was chosen long enough to suppress signal coming from bound water and short enough to minimize T_2 contrast. Nevertheless, there is still a small decrease in the signal of the lumen water due to transverse relaxation.

Magnetic resonance imaging acquisition consisted of three slices with an effective thickness of 2 mm and a 5 mm inter-slice distance (Fig. 2A and B). The total scan time for imaging acquisition was 3 min.

A glass tube (4.5 mm of internal diameter) containing 5 mM of copper sulfate dissolved in water was used as a reference image. Copper sulfate was used to shorten longitudinal relaxation times to a value of 100 ms and transverse relaxation time to 45 ms. The grey level obtained in water (1.8×10^6 arbitrary unit) allowed us to convert the grey levels of wood images into volumetric water content. For example, we found 1.3×10^6 (arbitrary unit) as density in saturated parts of earlywood. This corresponds to an apparent water density of 720 kg m^{-3}. Due to the short relaxation time of bound water, it was considered that the grey level includes only liquid water. Assuming that the bound water content at saturation and the cell-wall density are equal to 30% (dry basis) and 1500 kg m^{-3}, respectively (Siau, 1995), we obtain a basic wood density (oven-dry mass to green volume) in earlywood equal to 320 kg m^{-3}. This value agrees very well with literature data (Bosshard, 1984; Gartner et al., 2002). This is why a small application program was developed to convert the grey levels of each image in apparent specific gravity values. The same application allows the three slices to be saved in 3D data files using the Tecplot software.

2.1.3. Anatomical measurements

Duplicate samples were taken next, in longitudinal direction, to those used for the pressure membrane/MRI analysis. They were examined using an environmental scanning electron microscope (ESEM, FEI Quanta 200) located at INRA-ENGREF/Nancy. Uncoated samples were observed at a voltage below 10 kV and a chamber pressure of 1 Torr using a large field gaseous detector (secondary electrons). Cross-sectional images at different magnifications were taken in order to measure cell diameters and cell-wall thickness of earlywood, latewood, and ray parenchyma.

3. Results

Images obtained by MRI and ESEM are presented in Fig. 3A and B–D, respectively. The signal obtained in the MRI technique consists of mostly, if not entirely, liquid water (also called free water in wood science) present in the lumen of the wood specimen. As earlier cited, bound water and solid wood were not visible due to their rapidly decaying signal in contrast to the slowly decaying signal of the liquid water. In the MRI figures presented in this work, lighter colours mean higher liquid water content. The average moisture content (dry basis) was initially equal to 156% (CV of 1%) and 110% (CV of 4%) at the end of the experiment (average of three tests realized on longitudinal direction).

Due to their differences in anatomical structure, earlywood and latewood areas are easily distinguished in the NMR images (Fig. 3A). Earlywood presents thin cell walls and large lumen diameters, whereas latewood has thick cell walls and small lumen diameter (Fig. 3B and C). The decay signal for liquid water in the cell lumens has been found to be roughly proportional to the cell lumen diameter on different wood species (Menon et al., 1987; Flibotte et al., 1990; Almeida et al., 2007). Fig. 3A, B and D also exhibit

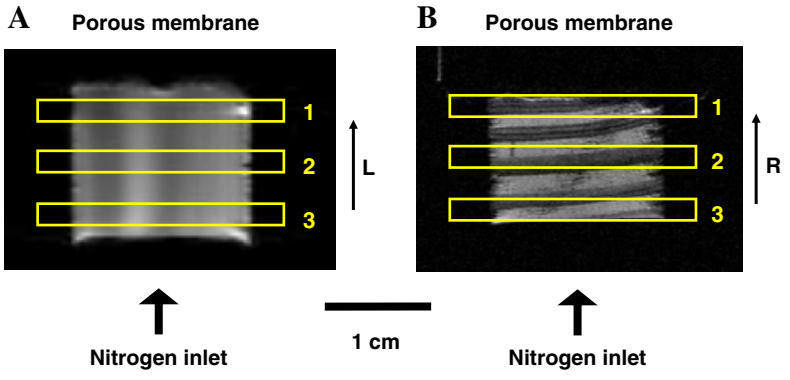

Fig. 2. Configuration of the specimens inside the pressure chamber showing the flow direction and slice position of MRI acquisition: (A) longitudinal flow and (B) radial flow.

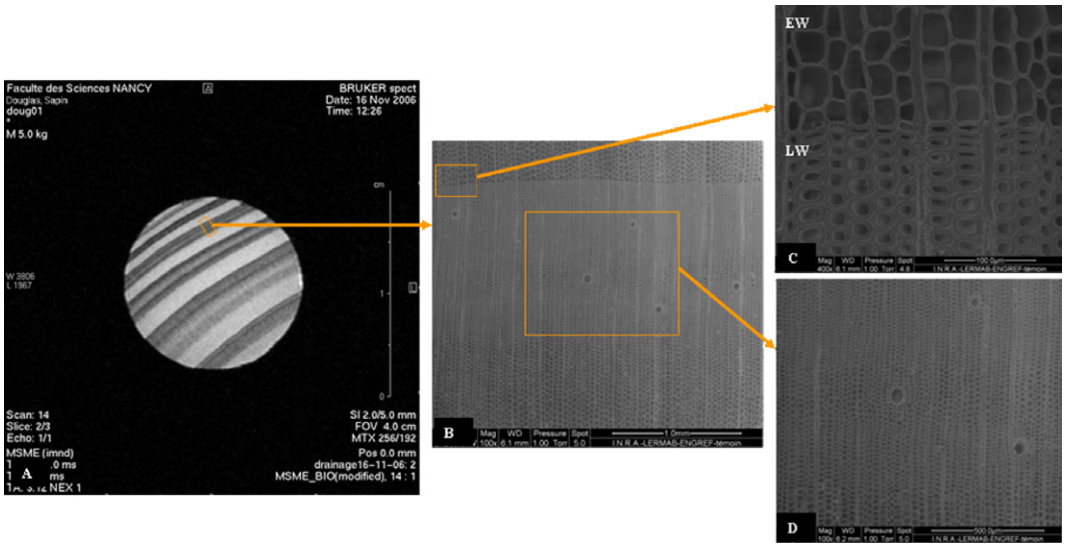

Fig. 3. Transversal section images of Douglas fir specimen. (A) NMR image showing dark latewood and light coloured earlywood. (B–D) ESEM micrographs: (B, C) earlywood (EW) and latewood (LW) zones and (D) irregularity of cell diameters in the latewood zone (false growth ring).

false rings within annual growth rings. They correspond to a pause in secondary growth rate due to climatic conditions, such as drought.

The evolution of water drainage in the longitudinal direction is shown in Fig. 4. These raw data represent the signal intensity in the three slices at different drainage

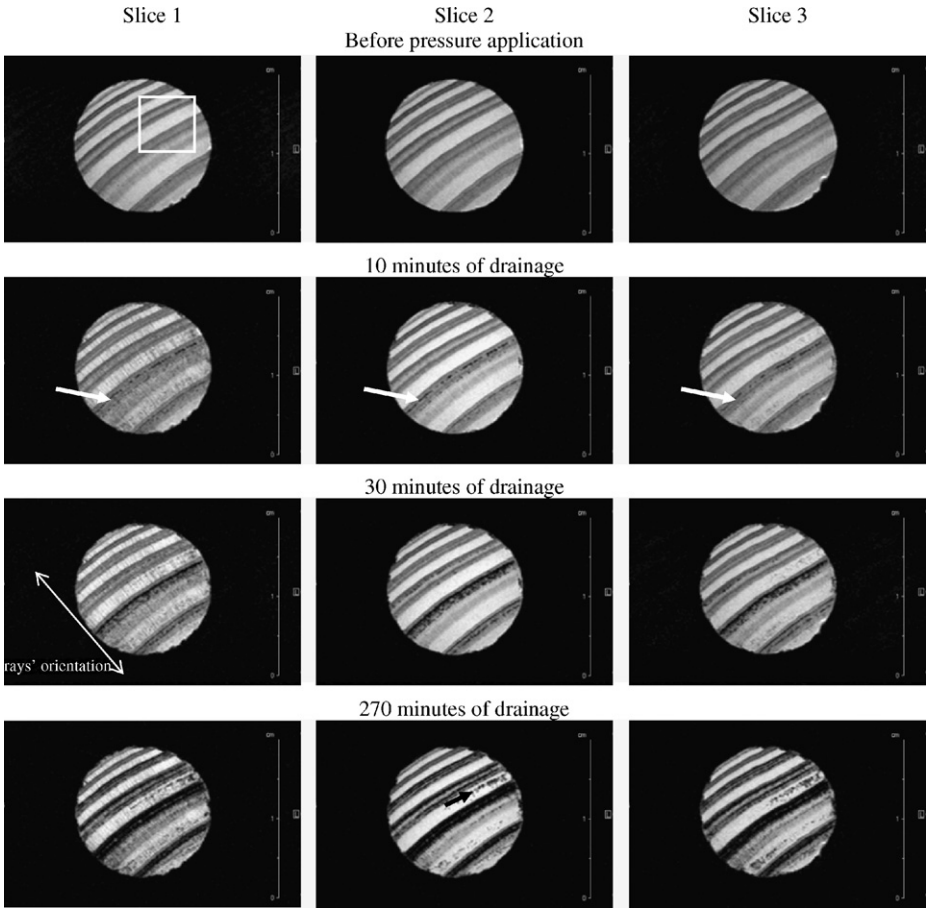

Fig. 4. Evolution of water drainage (longitudinal flow) in three slices of the specimen. White arrows indicate percolation spots in the latewood zone. The black arrow depicts the beginning of drainage clusters in earlywood at the end of the experiment. The white square (top left) is the magnified zone exhibited in Fig. 5.

times. Ten minutes after the pressure was applied, first drainage spots (dark areas) can be observed on one of the latewood rings. It should be notice that these drainage spots can be observed on the three slices (along the specimen), showing the flow connectivity in the latewood tracheids. These drainage zones then spread in the transverse plane until coalescence occurred (30 min). At this time, the water proportion in earlywood remains unchanged. This is surprising because this part of the annual ring is reputed to have a much higher permeability than the latewood part. At the end of the experiment (270 min) all latewood parts are fully drained. At this time, some drainage spots just start to be visible in one of the earlywood zones.

A better representation of these experimental data is proposed in Fig. 5. The views depicted in Fig. 5 consist of three slices (flood contours of five values regularly spread from 0.12 to 0.68 for the apparent specific gravity of liquid water) plus one 3D isovalue (0.12), which allows the shape of the drained zones to be pictured. For the sake of visibility, the cut-off colour possibility proposed by Tecplot was activated: zones below 0.12 are not coloured in the slices.

Fig. 5 shows that before pressure is applied, the three slices are similar, where a high water content difference between earlywood (0.6–0.8) and latewood (0.3–0.5) is evident. After 10 min of drainage, the water content field had already decreased significantly in the earlywood zones of slice 1, where the pressure is applied. Thin fingerings are obvious throughout the sample length in one latewood zone. The 0.12 isovalue surface proves that the drained spots observed on the images are perfectly aligned along the longitudinal direction of the wood.

At 20 min, no clear evolution was noticed, except that the narrow fingers had time to spread and now tend to coalesce in the transverse plane. This tendency is confirmed after 1 h of drainage: at this time, the latewood zone of this

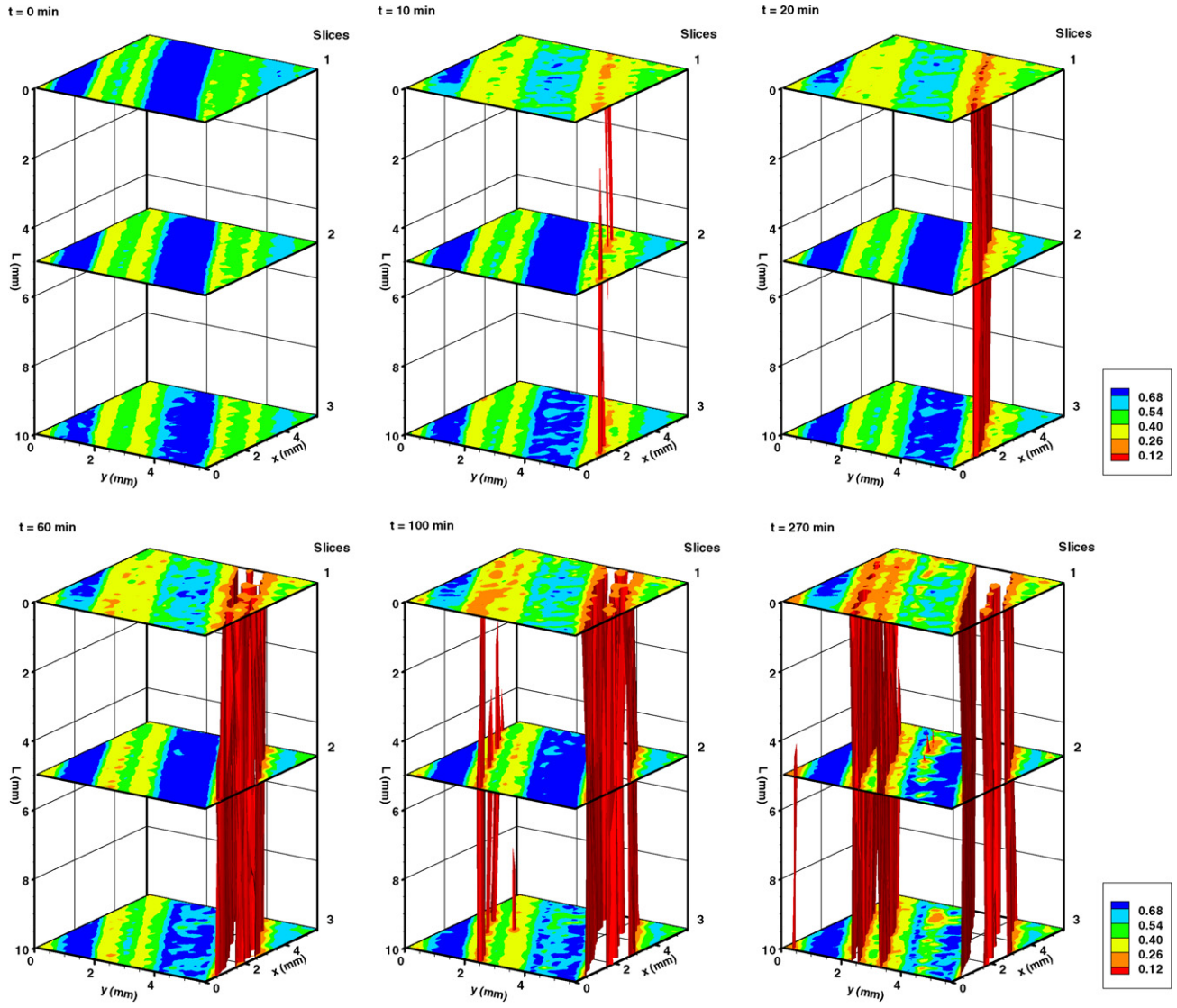

Fig. 5. Three-dimensional MRI of the apparent specific gravity of water at six different drainage times. This magnified zone is specified by a square in Fig. 4 (top left).

annual ring lost almost all its liquid water content. However, isolated water clusters appeared: they remained up to the end of the experiment. Although the time required for the second latewood zone to be drained is longer (100 min), the mechanism seems to be identical, with the appearance of narrow fingers spreading throughout the sample length.

At the end of the test (270 min), the two latewood zones present a bimodal pattern, with isolated water clusters existing inside a fully drained zone. In the second latewood zone, these water clusters remain connected in the tangential direction, along the false ring. At this time, one earlywood zone just started to be drained. Again, the drainage mechanism seems to be identical, with the existence of narrow spots. Even though they are not yet entirely connected in the longitudinal direction, the contour patterns of the different slices prove that the longitudinal connection indeed exists.

As discussed above, the first clusters of drainage are observed in the same latewood ring. These first drainage clusters and a magnification of the latewood ring can be observed in Fig. 6A and B, respectively. Some irregularities in the diameter of the latewood tracheids (false latewood ring) are also observed in Fig. 6B. Analyzing these figures, one can observe that the percolation network starts on the latewood tracheids of larger diameters, which are more permeable than the smaller ones.

The longitudinal drainage also gives us information about the drainage of ray parenchyma (Fig. 4, slice 1). This drainage is only observed in slice 1, where the cut rays on the surface of the sample are exposed to the nitrogen inflow. Slice 1 (Figs. 4 and 5) also shows that the earlywood exposed to nitrogen inflow has less liquid water than the earlywood of slices 2 and 3.

The results of water drainage in the radial direction are presented in Fig. 7A (before pressure application), B (10 min after a pressure application of 500 kPa) and C (80 min after pressure application). Even if this experiment favoured radial flow, comparison between these figures shows superficial flow along the tracheids (longitudinal direction) and homogenization of humidity inside the sample. After 80 min of experiment, the radial drainage is not observed. Several works have reported the ray parenchyma as being the least permeable tissue in the wood structure

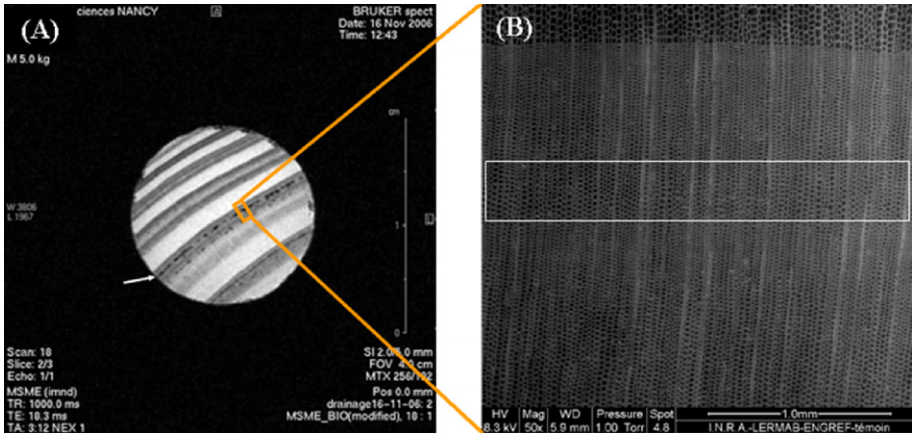

Fig. 6. Transversal section of Douglas fir. (A) MRI showing the first percolation network (white arrow). (B) ESEM micrograph (the box highlights the region where the first percolation network was observed).

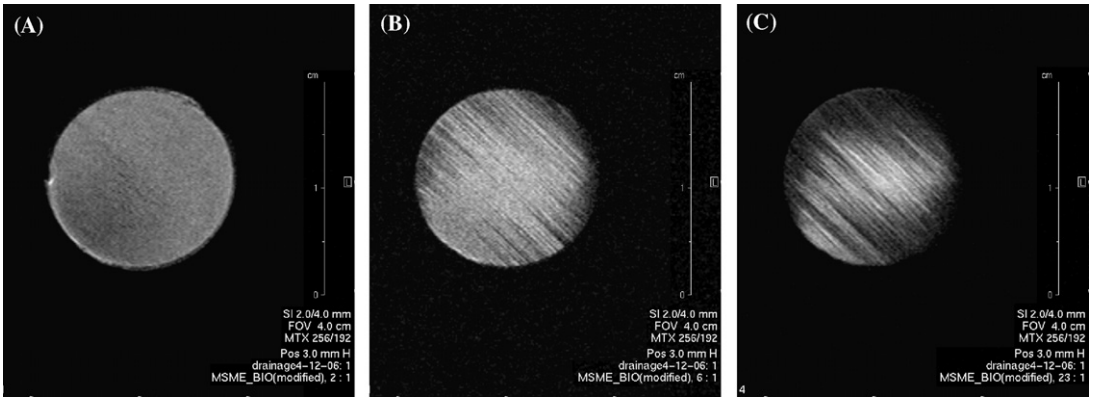

Fig. 7. Tangential–longitudinal section of Douglas fir (radial flow). (A) MRI before pressure application (slice 2). (B) MRI after 10 min of pressure application (slice 2). (C) MRI after 80 min of pressure application (slice 2).

(Hart et al., 1974; Gonzalez and Siau, 1978; Wheeler, 1982; Siau, 1995; Almeida and Hernández, 2006), Fig. 7 corroborates results of these works.

4. General discussion

4.1. Drainage of latewood and earlywood

The results presented in Figs. 4 and 5 definitely prove that the easiest pathway for drainage is in latewood. At first glance, this is surprising because it is well known that earlywood is the most permeable part of softwoods in the case of single phase flow. Another feature of fluid flow in wood has therefore to be considered to explain our observations. According to the cohesion-tension theory, the driving force that induces the ascent of sap in tree is generated by the surface tension at the evaporating surfaces of the leaf, in the stomata (Tyree, 1997). Because most trees are more than 10 m high, one can deduce that the absolute liquid pressure in the sap column is negative. No gaseous phase can exist in such conditions, which renders this sap column very fragile. Indeed, the vascular system is such that the tree must be able to support a gas invasion due to injury or cavitation. In softwoods, this is the role of bordered pits. These bordered pits are specialized valves: in the case of single-phase flow (sap flow) they are permeable, but they close off (this is called pit aspiration) by capillary forces when a liquid/gas meniscus passes through it. In latewood, the small and thick membranes (torus) and strands of the bordered pits might not allow them to act as a valve. Indeed, the low resistance of latewood zones to embolism in the living tree and the higher drainage of these zones in the wood are a consequence of the structural features of the bordered pit membrane: low pit diameter and large cell-wall thickness in latewood compared to earlywood (Bolton and Petty, 1978; Panshin and de Zeeuw, 1980; Perré and Turner, 2001; Domec and Gartner, 2002; Usta, 2005).

4.2. Capillary regime

Drainage consists of the immiscible displacement of a wetting fluid by a non-wetting fluid. In this configuration, capillary forces act against the flow. For slow displacements (capillary regime), capillary forces prevail and the front shape is controlled by the heterogeneity of the pore sizes along the interface. When the displacing fluid is less viscous than the displaced fluid, viscous forces destabilize the interface as the flow rate increases (viscous regime). The capillary number Ca can be used to distinguish these two regimes. This number is usually expressed as follows (Dullien, 1992):

$$\mathrm{Ca} = \frac{\text{Viscous forces}}{\text{Capillary forces}} = \frac{v\mu_w}{\sigma\cos\theta} \tag{3}$$

where v and μ_w are the velocity and viscosity, respectively, of the wetting fluid; σ is the water–gas interfacial tension and θ is the contact angle (0° here because water perfectly wets the wood substance).

Finally, gravity can also stabilize or destabilize the interface, but its effect can be discarded in our experiments because the main flow is horizontal and the sample depth involves a very small pressure difference in comparison with the applied pressure.

In our experiment of wood drainage by nitrogen, it is not obvious whether fingering results from a viscous regime or a capillary regime. Our viscous ratio ($\kappa = \mu_w/\mu_{nw} \approx 50$ at 20 °C) and the rapid breakthrough of the non-wetting fluid into the wetting fluid suggest that a viscous regime could take place (Lenormand et al., 1988). Calculating Ca needs the velocity to be evaluated. Two methods could be used:

- to evaluate the fluid velocity of the active pores (about 10 min for the first fingers to cross the 20 mm sample length): $v_1 = 3.3 \times 10^{-5}$ m s^{-1},
- to consider the initial velocity (single fluid phase and intrinsic permeability) using Darcy's law. Assuming the longitudinal permeability in Douglas fir to be 10^{-13} m^2 and its porosity 0.66, we obtain $v_2 = 2.5 \times 10^{-3}$ m s^{-1}.

In fact, v_2 is certainly overestimated, firstly because the calculation neglects the resistance due to the membranes and the clay layer, and because a multiphase flow configuration takes place as soon as the experiment starts. Relative permeability factors should be added, that reduces considerably the medium permeability to each fluid phase.

Retaining value v_1, the capillary number, Ca, is equal to 4.5×10^{-8}. Referring, with care, to the literature data (Lenormand et al., 1988), this value seems too low to produce viscous fingering. It seems, therefore, that capillary fingering is responsible for the thin fingers observed here. The fact that the drainage of the second latewood zone, then of the first earlywood zone, presents similar patterns (Fig. 5), is an additional argument in the favour of capillary fingering. These zones are indeed drained over a much longer period, which reduces the capillary number by more than one order of magnitude.

The long and narrow shape of fingers is therefore certainly due to the strong anisotropy of wood: crossing one pit allows the flow to progress about 3 mm in the longitudinal direction and only about 30 μm in the cross-sectional plane. Once a pathway exists along the sample length, it allows gradual transverse drainage, from one tracheid to its neighbour: one open pit is enough for this lateral drainage, instead of at least two (one at each cell end) for longitudinal migration. Finally, entrapped water clusters can be analyzed as groups of tracheids without unaspirated pits.

During most of the experimental time, earlywood zones seemed to be completely impervious. This observation was analyzed due to the high proportion of aspirated pits in this part of the wood. Therefore, the late drainage of one earlywood zone denotes that, in spite of aspiration, the pits are

not perfectly impervious. Some leakage does exist, namely in minute opening that continue to exist in aspirated pits, between the torus and the cell wall. The applied pressure (500 kPa) is able to force the meniscus to pass through in pores whose radius is above 0.288 μm (Eq. (2)).

5. Conclusion

A procedure was developed to visualize fluid flow through a porous media. This procedure combines two techniques, namely, NMR imaging and pressure membrane. Thus, the present work shows the displacement of the wetting phase by application of the non-wetting phase in Douglas fir samples. Earlywood and latewood are easily distinguished in the images obtained. The procedure presented in this work successfully shows the longitudinal flow inside a porous media. Clusters of drainage are first formed in the latewood zones, these clusters are longitudinally connected. Drainage zones in latewood increase until the coalescence. At the end of the experiments, the drainage of liquid water in the latewood is completed and few sites of percolation are observed in earlywood zones. This result is a consequence of the anatomical structure of wood, where earlywood pits are more easily aspirated than those of the latewood.

Acknowledgements

This work was supported by the State of São Paulo Research Foundation (FAPESP) and "Fédération de Recherche Jacques Villermaux". The authors are grateful to Professor Yves Fortin (Laval University, Quebec, Canada) for precious suggestions about the pressure membrane method and to Françoise Huber (LERMaB/INRA) for valuable advice about ESEM utilization. The authors would also like to thank the NMR service of Nancy I University for the use of the Bruker Biospec.

References

Almeida, G., Hernández, R.E., 2006. Changes in physical properties of yellow birch below and above the fiber saturation point. Wood Fiber Sci. 38, 74–83.

Almeida, G., Gagné, S., Hernández, R.E., 2007. A NMR study of water distribution in hardwoods at several equilibrium moisture contents. Wood Sci. Technol. 41, 293–307.

Araujo, C.D., MacKay, A.L., Whittall, K.P., Hailey, J.R.T., 1993. A diffusion model for spin–spin relaxation of compartmentalized water in wood. J. Magn. Reson. B 101, 248–261.

ASTM, 2000. D3152-72(2000) Standard Test Method for Capillary-Moisture Relationships for Fine-Textured Soils by Pressure-Membrane Apparatus. American Society for Testing and Materials, West Conshohocken, PA.

Bolton, A.J., Petty, J.A., 1978. A model describing axial flow of liquids through conifer wood. Wood Sci. Technol. 12, 37–48.

Bosshard, H.H., 1984. Holzkunde, Band: 2: Zur Biologie, Physik und Chemie des Holzes, Birkhäuser, Basel.

Chen, Q., Kinzelbach, W., Oswald, S., 2002. Nuclear magnetic resonance imaging for studies of flow and transport in porous media. J. Environ. Qual. 31, 477–486.

Core, H.A., Côté, W.A., Day, A.C., 1979. Wood Structure and Identification. Syracuse University Press.

Deurer, M., Vogeler, I., Khrapitchev, A., Scotter, D., 2002. Imaging of water flow in porous media by magnetic resonance imaging microscopy. J. Environ. Qual. 31, 487–493.

Domec, J.-C., Gartner, B.L., 2002. How do water transport and water storage differ in coniferous earlywood and latewood?. J. Exp. Botany 53 2369–2379.

Dullien, F.A.L., 1992. Porous Media: Fluid Transport and Pore Structure, second ed. Academic Press, San Diego, 574p.

Eberhardt, T.L., So, C.L., Herlihy, A.H., So, P.W., 2006. Use of gadolinium chloride as a contrast agent for imaging spruce knots by magnetic resonance. Wood Fiber Sci. 38, 527–534.

Flibotte, S., Menon, R.S., MacKay, A.L., Hailey, J.R.T., 1990. Proton magnetic resonance of western red cedar. Wood Fiber Sci. 22, 362–376.

Fortin, Y., 1979. Moisture content-water potential relationship and water flow properties of wood at high moisture contents. Thèse de Ph.D. Université de British Columbia, Vancouver, 187p.

Gartner, B.L., North, E.M., Johnson, G.R., Singleton, R., 2002. Effects of live crown on vertical patterns of wood density and growth in Douglas-fir. Can. J. For. Res. 32, 439–447.

Gonzalez, G.C., Siau, J.F., 1978. Longitudinal liquid permeability of American beech and eucalyptus. Wood Sci. 11, 105–110.

Griffin, D.M., 1977. Water potential and wood-decay fungi. Annu. Rev. Phytopathol. 15, 319–329.

Hart, C.A., Przestrzelski, P.J., Wheeler, F.J., 1974. Entrapped lumen water in hickory during desorption. Wood Sci. 6, 356–362.

Kimmich, R., Klemm, A., Weber, M., 2001. Flow, diffusion, and thermal convection in percolation clusters: NMR experiments and numerical FEM/FVM simulations. Magn. Reson. Imaging 19, 353–361.

Kuroda, K., Kanbara, Y., Inoue, T., Ogawa, A., 2006. Magnetic resonance micro-imaging of xylem sap distribution and necrotic lesions in tree stems. IAWA J. 27, 3–17.

Lenormand, R., Touboul, E., Zarcone, C., 1988. Numerical models and experiments on immiscible displacement in porous media. J. Fluid Mech. 189, 165–187.

Meder, R., Codd, S.L., Franich, R.A., Callaghan, P.T., Pope, J.M., 2003. Observation of anisotropic water movement in Pinus radiate D. Don sapwood above fiber saturation using magnetic resonance microimaging. Holz Roh Werkst. 61, 251–256.

Menon, R.S., Mackay, A.L., Hailey, J.R.T., Bloom, M., Burgess, A.E., Swanson, J.S., 1987. An NMR determination of the physiological water distribution in wood during drying. J. Appl. Polym. Sci. 33, 1141–1155.

Merela, M., Sepe, A., Oven, P., Serša, I., 2005. Three-dimensional in vivo magnetic resonance microscopy of beech (*Fagus sylvatica* L.) wood. Magma 18, 171–174.

Panshin, A.J., de Zeeuw, C., 1980. Textbook of wood technology. Structure, Identification, Properties and Uses of the Commercial Woods of the United States and Canada. McGraw-Hill, New York.

Perré, P., Turner, I., 2001. Determination of the material property variations across the growth ring of softwood for use in a heterogeneous drying model. Part I: capillary pressure, tracheid model and absolute permeability. Holzforschung 55, 318–323.

Quick, J.J., Hailey, J.R.T., MacKay, A.L., 1990. Radial moisture profiles of cedar sapwood during drying: a proton magnetic resonance study. Wood Fiber Sci. 22, 404–412.

Riggin, M.T., Sharp, A.R., Kaiser, R., Schneider, M.H., 1979. Transverse NMR relaxation of water in wood. J. Appl. Polym. Sci. 23, 3147–3154.

Robertson, A.A., 1965. Investigation of the cellulose–water relationship by the pressure plate method. Tappi 48, 68–573.

Siau, J.F., 1995. Wood: Influence of Moisture on Physical Properties. Virginia Polytechnic Institute and State University, VA, 227p.

Stone, J.E., Scallan, A.M., 1967. The effect of component removal upon the porous structure of the cell wall of wood. II. Swelling in water and the fiber saturation point. Tappi 50, 496–501.

Tyree, M.T., 1997. The cohesion-tension theory of sap ascent: current controversies. J. Exp. Botany 48, 1753–1765.

Usta, I., 2005. A review of the configuration of bordered pits to stimulate the fluid flow, Maderas. Cienc. Technol. 7, 121–132.

van Houts, J.H., Wang, S., Shi, H., Pan, H., Kabalka, G.W., 2004. Moisture movement and thickness swelling in oriented strandboard, part 1. Analysis using nuclear magnetic resonance microimaging. Wood Sci. Technol. 38, 617–628.

Waggoner, R.A., Fukushima, E., 1996. Velocity distribution of slow fluid flows in Bentheimer sandstone: an NMRI and propagator study. Magn. Reson. Imaging 14, 1085–1091.

Wheeler, E.A., 1982. Ultrastructural characteristics of red maple (*Acer rubrum* L.) wood. Wood Fiber Sci. 14, 43–53.

Williams, J.L.A., Taylor, D.G., Maddinelli, G., Enwere, P., Archer, J.S., 1991. Visualization of fluid displacement in rock cores by NMR imaging. Magn. Reson. Imaging 9, 767–773.